Towards Reconfigurable Optical Metamaterials: Colloidal Nanoparticle Self-Assembly and

Hybrid nanostructured materials based on nanoparticles and liquid crystals (LCs) are a class of composites poised to revolutionize scientific instruments, technologies, and devices, and may enable self-assembly-based approaches for fabrication of metamaterials [15]. LCs may enable reconfigurable and switchable self-assembly of dispersed nanoparticles directed by the nanoscale molecular ordering in these anisotropic fluids with a broad range of mesomorphic phases. Control of the colloidal and molecular structural organization and ensuing composite properties may be achieved by using intrinsic liquid crystalline self-assembly and

are needed to further the collective understanding of these media on the nanoscale. Therefore, motivating this work with the current state-of-the-art of nanoscale LC imaging is a convincing way of presenting the importance and the need for the development of optical metamaterials. Figure 1 shows nanoscale images of a chromonic lyotropic LC obtained by a cryogenic transmission electron microscope (TEM), a powerful nanoscale imaging technique that is rarely available to researchers. Because of the need to freeze the samples and a number of other limiting factors, this technique is incapable of revealing the dynamics of the nematic and columnar hexagonal ordering of the constituent molecular stacks. Despite of the recent interest in the lyotropic chromonic LCs, they remain poorly understood, and even the types of molecular organization into chromonic stacks still need to be clarified for some of

3. Materials and Experimental Techniques

3.1. Synthesis of Gold Nanoparticles

Although gold nanoparticles have been used in red stained glass in cathedrals for centuries and have been studied extensively starting from the works by Faraday, their potential use in metamaterials requires a precise control of particle shapes and their spatial structuring on length scales much smaller than the wavelength of visible light. This sets new fundamental research and engineering challenges from the standpoint of their synthesis, dispersion, and controlled structural organization. The synthesis of colloidal gold nanoparticles typically occurs through the reduction of gold cations in the presence of a certain capping agent. The size and shape of the nanoparticles are determined by the kinetics of nucleation, the ratio of gold and capping agent, and the stabilization of different crystallographic faces by the capping agents [61]. To produce spherical particles, fast reduction with no preferential surface stabilization is ideal. For example, in the Brust-Schiffrin method, chloroauric acid is complexed with tetraoctylammonium bromide (TOAB) and toluene to enter the organic phase [62]. It is then reduced by sodium borohydride in the presence of excess thiol to produce 2 nm spheres (Fig. 3a). If no thiol is added, TOAB stabilizes the formation of 20 nm spheres (Fig. 3b).

The growth of non-spherical nanoparticles requires slower reduction and preferential selection of crystal facets. One of the best known examples of synthesis of non-spherical metal nanoparticles is the synthesis of nanorods capped by cetyl trimethylammonium bromide (CTAB) [63,64]. In the synthesis procedure, spherical seeds are produced by reducing chloroauric acid with sodium borohydride in the presence of sodium citrate or CTAB. These spherical seeds are then transferred to

Figure 3. Examples of nanoparticles of different material composition, shapes, and sizes. a) Gold nanospheres of 2–3 nm in diameter. b) gold spheres of 20 nm in diameter. c) CTAB capped gold nanorods with an aspect ratio of about 3. d) CTAB capped gold nanorods with aspect ratios ranging from 15 to 20. e) dog-bone-shaped gold nanoparticles. f) PVP capped silver triangle synthesized by photoreduction. g) CdSe quantum rods with aspect ratio of about 2. h) short gold nanorods obtained from NanoPartz.

a growth solution with more CTAB, chloroauric acid, and ascorbic acid that produces a mild reduction on the $<110>$ facets of the seed particles [65] (Fig. 3c,d). If the ascorbic acid is too active, then the ends can get overgrown producing anisotropic nanoparticles with shapes resembling ''dog bones'' [66] (Fig. 3e). Triangular platelets can be synthesized using various methods such as photoreduction (Fig. 3f) [67] and biosynthesis [68]. These triangles and dog bones mentioned above are of

dispersion quality (i.e., absence of micron-scale or larger nanoparticle aggregates) is assessed by means of the transmission-mode bright-field imaging. The phase behavior and LC alignment is studied by the same microscope in the polarizing optical imaging mode using 10×, 20×, and 50× air objectives (all from Olympus) with numerical aperture NA = 0.3–0.9 as well as a Spot 14.2 Color Mosaic Camera (from Diagnostic Instruments, Inc.). In addition, we have used an inverted microscope IX81 with a fluorescence attachment, a confocal microscopy scanning unit, and a NA = 1.4 objective (all from Olympus). The SPR extinction spectra are measured using a USB-2000 microspectrometer (Ocean Optics) mounted on the optical microscope.

3.4. Nanoscale Imaging of Nanoparticles in Liquid Crystals

The images of the synthesized nanoparticles, such as those shown in Figure 3, are obtained using a Philips CM10 TEM (FEI, Inc.) operating at 80kv. However, regular TEM is not appropriate for probing the structural assembly and alignment of nanoparticles in LCs because, in addition to many other reasons, the vacuum levels at which the conventional TEM operates cause LC evaporation. To overcome this problem, and to get insights into the nanoscale structural assembly in nanoparticle-doped LCs, we use a technique known as Freeze Fracture Transmission Electron Microscopy (FFTEM) that has been widely used in the studies of LCs.

The sample preparation for FFTEM imaging starts by taking a small quantity (2–4 μl) of the sample and sandwiching it between two thin copper substrates. This sample between the copper plates is then rapidly quenched in liquid propane to temperatures below −183°C. The copper sandwich is loaded into a BalTec freeze etch machine at a temperature of −140°C and pressure of 10^{-6} mbar. The copper sandwich is then fractured in the cold vacuum. The exposed fractured surfaces are shadowed with ∼2 nm of a platinum-carbon (Pt-C) alloy at 45° and ∼30 nm of carbon normal to the fractured plane. The Pt-C alloy is deposited for image contrast and the layer of carbon is used to improve mechanical stability. The shadowed sample is removed from vacuum, and gradually warmed to room temperature. It is then washed in deionized water, ethanol, and ethyl acetate to remove the LC host and nanoparticles leaving behind Pt-C replicas of the fracture plane. The Pt-C replicas are imaged using the TEM revealing the structural assembly and alignment of nanoparticles in the LC at the fractured plane. We also used an alternative method of FFTEM sample preparation. In this method, a sample of volume ∼2–4 μl is placed in a small copper bowl instead of sandwiching it between two copper plates. The sample in the bowl is frozen and inserted into the freeze etch machine as described above. Fracturing of the frozen sample is then done with a special knife. The rest

confocal polarizing microscopy. We explore the behavior of nanoparticles as the LC sample is subjected to temperature changes causing phase transitions. To perform these experiments, the dispersion of QDs in hexane is added to a commercial thermotropic nematic mixture E7 (EM Chemicals) at a concentration of 0.001% by weight. The cell with the QD-E7 dispersion is then placed into an Instec STC200 heating stage mounted on a fluorescent microscope. A 10x objective is used with a 488 nm argon laser to obtain monochromatic transmission optical microscopy images

isotopic-nematic phase boundary as long as possible, until the isotropic region of the sample disappears. This expulsion often leads to the transition-induced aggregation of colloidal inclusions. Furthermore, this clearly demonstrates that dispersion of nanoparticles in LC fluids is more challenging as compared to the isotropic solvents and even the nanoparticles that disperse well in isotropic melts of certain materials may aggregate as a result of a transition to the mesophase.

4.2. Expulsion of Fluorescent Nanoparticles to Confining Substrates

Partial expulsion of nanoparticles from the LC hosts is also observed for samples deep in the nematic phase. After being kept for several hours in the nematic LC, the fluorescent QDs partially segregate to the nematic-glass interface. The same

4.4. Improving the Stability of Cholesteric Blue Phases Using Nanoparticles

The feasibility of using periodic networks of defects in blue phases (BPs) as a template for spatial patterning of nanoparticles is explored by use of several different

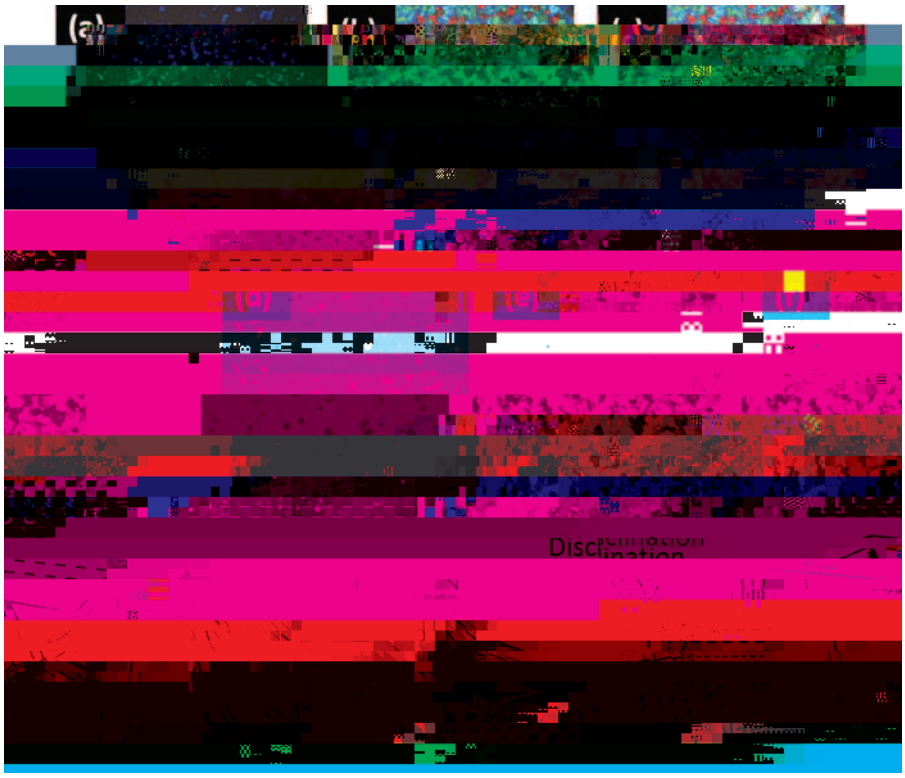

Figure 6. Effect of nanoparticle doping on the stability of the cholesteric blue phase. a-c) the textures of undopped sample cooled from isotropic to cholesteric phase at 0.1C/min. d–f) The textures of nanorod-doped blue phase as the mixture is cooled from isotropic to cholesteric phase at the same rate; the used gold nanorods are shown in Figure 3 h. g) double twist cylinder with the LC molecules aligned along the cylinder axis in its center and twisting in all radial directions when moving away from the center. h) 3D packing of the double twist cylinders into cubic lattices gives rice to disclination defects that form distinct 3D periodic networks in blue phases I and II. i) Nanorods are expected to localize in the defect cores and align along the disclinations. (Figure appears in color online.)

compositions, sizes, and shapes. Since the defect lattices in BPs can have periodicity of 100–200 nm, this spatial patterning is potentially useful for the self-assembly of metamaterials and other novel composite materials.

4.5. Direct Nanoscale Imaging of Well-Dispersed Nanoparticles in Liquid Crystals

To demonstrate that certain types of nanoparticles can disperse in the ground-state samples of LCs without aggregating or localizing into defects, we perform FFTEM imaging of the TI-827 doped with gold nanospheres (shown in Fig. 3b) at 10% concentration by weight. Figure 7a,b shows the FFTEM image of the sample having 300 nm pitch with the nanoparticles well-dispersed in the LC, as clearly seen from the high-magnification inset of the same area in the sample. Similar high-quality dispersion of the nanoparticles is seen throughout the sample except in a few areas

(Fig. 7c) where local aggregation may be ‘‘seeded’’ by much larger nanoparticles. The larger nanoparticles create stronger distortions in the LC molecular alignment that may trap surrounding nanoparticles to reduce the elastic distortion costs. Further experiments are needed to investigate how nanoparticle dispersions depend on particle size distribution.

4.6.

The enhanced aggregation of nanoparticles in the LC hosts is often facilitated by the elasticity-mediated inter-nanoparticle interactions. Studies of colloidal micro-particles in nematic LCs reveal strongly anisotropic long-range interactions that can be of both attractive and repulsive nature [73,74]. These interactions typically depend on topological defects and director distortions occurring around the particles and are mediated by orientational elasticity of the surrounding LC. In the case of micron-sized inclusions embedded in a nematic LC, both dipolar and quadrupolar configurations can occur, depending on the surface anchoring. When the orientation of the ''easy axis'' of the director is normal to the surface of the par-

interactions are weak, nanoparticle orientation with respect to the LC director can be controlled and depends on the symmetry of nanoparticle shape, its surface treatment, and the mesophase of the LC host [15,31].

The very same nanoparticle-induced elastic distortions that make their colloidal stabilization more difficult compared to that in isotropic fluids can be utilized for the controlled spatial patterning of nanoparticles. The nanoinclusion-induced distortions give rise to the elasticity-mediated interactions of the particles with defects and other distortions that can be deliberately induced by external fields and beams of light or pre-defined by ground states of certain phases, such as blue phases. The oily streak defects in the cholesteric phase, for example, attract the surrounding CdSe nanoparticles (Fig. 5), so that the defects in the doped samples strongly fluoresce, giving direct evidence for the location of particles in the defect cores (with the majority being concentrated in the defect nodes). Because of the existing network of defect lines in BPs, the nanorods can spatially localize into the defect cores, thus reducing the overall free energy by eliminating the energetically-costly regions of the disclination cores and sharing the distortions around nanorods with those due to defects. This not only allows for the nanoscale positioning of nanoparticles into the periodic three-dimensional network of defects cores but also for another practically useful effect, the increase of the temperature range of the BP existence (Table 1). Similar stabilization effect has been observed for various other types of nanoparticles, both experimentally and theoretically

6. Conclusions

In conclusion, we have demonstrated dispersion, self-alignment, and self-assembly of plasmonic metal nanoparticles in liquid crystals. Since the LC-mediated alignment and assembly of plasmonic nanoparticles gives rise to a switchable polarization-sensitive plasmon resonance (exhibiting stark differences from that of the same nanoparticles in isotropic fluids [15]), the LCs with self-assembled and self-aligned anisotropic nanoparticles are of interest for fabrication of tunable optical metamaterials. Furthermore, once the understanding and control of the underlying physical processes are improved, the device-scale bulk nanoparticle self-alignment and self-assembly may enable optical metamaterial mass production and control of their properties arising from combining the switchable nanoscale structure of LCs and the surface plasmon resonance properties of the plasmonic nanopartricles.

Acknowledgment

This work was supported by the Renewable and Sustainable Energy Initiative and Innovation Initiative Seed Grant Programs of University of Colorado at Boulder, International Institute for Complex Adaptive Matter, and by NSF grants DMR0645461, HRD0639653, DMR0820579, and DMR0847782. D.G. was supported by the SMART undergraduate research program of the Colorado Diversity Initiative. We thank Paras Prasad and Ken-Tye Yong for providing quantum dots and rods used in our studies. We thank Richard Gursky for discussions and for his help with obtaining the cryogenic TEM images of the chromonic LC samples. We also thank Corinne Beier, Budhadipta Dan, Clayton Lapointe, Qingkun Liu, Angel Martinez, Hector Mireles, Ramarao Pratibha, Sabrina Thompson, Rahul Trivedi, Christopher Twombly, and Bethany Wilcox for discussions and various assistance at different stages of this project.

References

[1] Veselago, V. G. (1968). *Soviet Physics Uspekhi, 10*, 509.
[2] Pendry, J. B. (2000). *Phys Rev. Lett.*, , 3966.
[3] Werner, D. H., Kwon, D. H., Khoo, I. C., Kildishev, A. V., & Shalaev, V. M. (2007). *Optics Express, 1* , 3342.
[4] Minovich, A., Neshev, D. N., Powell, D. A., Shadrivov, I. V., & Kivshar, Y. S. (2010). *Appl. Phys. Lett.*, , 193103.
[5] Soukoulis, C. M., Linden, S., & Wegener, M. (2007). *Science, 1* , 47.
[6] Li, T., Li, Y. Q., Wang, F. U., Wang, Q. J., Liu, H., Zhu, S. N., & Zhu, Y. Y. (2007). *Appl. Phys. Lett., 0*, 251112.
[7] Valentine, J., Zhang, S., Zentgraf, T., Ulin-Avila, E., Genov, D., Bartal, G., & Zhang, X. (2008). *Nature*, , 376.
[8] Kim, E., Wang, F., Wu, W., Yu, Z., & Shen, Y. R. (2008). *Phys. Rev. B.*, , 113102.
[9] Minovich, A., Neshev, D. N., Powell, D. A., Shadrivov, I. V., Lapine, M., McKerracher, I., Hattori, H. T., Tan, H. H., Jagadish, C., & Kivshar, Y. S. (2010). *Phys, Rev. B.*, *1*, 115109.
[10] Zhang, S., Fan, W., Panoiu, N. C., Malloy, K. J., Osgood, R. M., & Brueck, S. R. J. (2005). *Phys. Rev. Lett.*, , 1347404.
[11] Dolling, G., Enkrich, C., Wegener, M., Soukoulis, C. M., & Linden, S. (2006). *Science, 12*, 892.

[45] Zhang, S., Leem, G., Srisombat, L., & Lee, T. R. (2008). *J. Am. Chem. Soc.*, *1 0*, 113.
[46] Halle, B., Quist, P. O., & Furó, I. (1992). *Phys. Rev. A*,¶ , 3763.
[47] Wu, K. J., Chu, K. C., Chao, C. Y., Chen, Y. F., Lai, C. W., Kang, C. C., Chen, C. Y., & Chou, P. T. (2007). *Nano Lett.*, , 1908.
[48] Yong, K. T., Sahoo, Y., Swihart, M., & Prasad, P. (2006). *Advanced Materials*, *1* , 1978.
[49] Yoshida, H., Tanaka, Y., Kawamoto, K., Kubo, H., Tsuda, T., Fujii, A., Kuwabata, S., Kikuchi, H., & Ozaki, M. (2009). *Applied Physics Express*, *2*, 121501.
[50] Lydon, J. (1998). *Current Opin. Colloid & Interface Sci.*, , 458.
[51] Kachynski, A. V., Kuzmin, A. N., Prasad, P. N., & Smalyukh, I. I. (2008). *Optics Express*, *1* , 10617.